

# Small Planetesimals in a Massive Disk Formed Mars

Hiroshi Kobayashi

Department of Physics, Graduate School of Science, Nagoya University, Furo-cho,  
Chikusa-ku, Nagoya 464-8602, Japan

hkobayas@nagoya-u.jp

Nicolas Dauphas

Origins Laboratory, Department of the Geophysical Sciences and Enrico Fermi Institute,  
The University of Chicago, 5734 South Ellis Avenue, Chicago, Illinois 60637, USA

dauphas@uchicago.edu

**Icarus, 225, 122**

Received \_\_\_\_\_; accepted \_\_\_\_\_

## ABSTRACT

Mars is likely to be a planetary embryo formed through collisions with planetesimals, which can explain its small mass and rapid formation timescale obtained from  $^{182}\text{Hf}$ - $^{182}\text{W}$  chronometry. In the classical theory of planet formation, the final embryo mass is determined only by the solid surface density. However, embryos can stir surrounding planetesimals, leading to fragmentation through erosive (cratering) collisions. We find that radial drift of small fragments can drastically reduce the solid surface density. On the other hand, embryo growth is accelerated by fragment accretion. Since collisional fragmentation efficiency depends on the initial size of planetesimals, the final embryo mass and its growth time are determined by the initial planetesimal size and disk surface density. We have investigated the effect of these two parameters on the mass of Mars and the predicted radiogenic excess of  $^{182}\text{W}$  in the martian mantle. Two scenarios can explain the rapid formation of small Mars: (i) it formed by accretion of small planetesimals in a massive disk or (ii) it formed from large planetesimals but its growth was arrested by the inward then outward migration of Jupiter. Taking into account all constraints, we conclude that Mars is likely to have formed in a massive disk of about  $\sim 0.1$  solar mass from planetesimals smaller than  $\sim 10$  km in radius. Such small planetesimal size cannot explain core accretion of Jupiter, suggesting that there may have been a heliocentric gradient in planetesimal size in the solar nebula.

Key Words: Mars; terrestrial planets; planetary formation; planetesimals; origin, solar system

## 1. INTRODUCTION

Mars, one of four terrestrial planets in the solar system, has a small mass of  $0.11 M_{\oplus}$  ( $M_{\oplus}$  = Earth mass) and an orbital semimajor axis of 1.5 AU. Terrestrial planets are believed to have formed via collisions among Mars-sized planetary embryos in the long-term orbital instability that followed substantial gas dissipation (*i.e.*, chaotic growth; Chambers et al. 1996; Iwasaki et al. 2001; Kominami and Ida 2002; Kenyon and Bromley 2006; Ogihara et al. 2007). The  $^{182}\text{Hf}$ - $^{182}\text{W}$  short-lived chronometer ( $t_{1/2} = 9$  Myr) gives a very short accretion timescale for Mars (Dauphas and Pourmand 2011), similar to the gas dissipation time inferred from disk and meteorite observations (Dauphas and Chaussidon 2011; Haisch et al. 2001). This indicates that Mars is likely to be a remnant of the early generation of planetary embryos formed via collisional accretion of planetesimals.

Collisions between planetesimals produced planetary embryos, which grew further through collisions with surrounding planetesimals (Wetherill and Stewart 1993; Weidenschilling et al. 1997; Kokubo and Ida 1998). Once embryos became massive, they stirred surrounding planetesimals, producing collisional fragments that contributed to embryo growth (Wetherill and Stewart 1993; Inaba et al. 2003; Chambers 2006, 2008; Kenyon and Bromley 2004, 2009; Ormel and Kobayashi 2012). When the surrounding bodies were depleted due to the radial drift of small fragments and/or accretion onto embryos, the growth of embryos stalled (Kobayashi et al. 2010). In oligarchic growth, the initial size of planetesimals and disk mass influence the final masses of embryos and their accretion timescales. Small planetesimals are easily fragmented during collisions. The resulting fragments are small enough to feel some drag from the gas, leading them to spiral towards the Sun. As a result, small planetesimals tend to produce embryos that have smaller masses than when large initial planetesimals are considered. On the other hand, the interaction of fragments with the gas damps their relative velocities and increases the

efficiency with which they can be accreted by embryos through gravitational focusing. Thus, with small planetesimals the timescale of embryo growth is shorter than when large planetesimals are considered.

During formation of the terrestrial planets, the segregation of metal from silicate produced metallic cores, the timing of which can be estimated using  $^{182}\text{Hf}$ - $^{182}\text{W}$  systematics. Hafnium, a lithophile (i.e., rock-loving) element, was retained. In contrast, tungsten, a siderophile (i.e., metal-loving) element, was partitioned into metal cores. Hafnium-182 ( $^{182}\text{Hf}$ ) decays to tungsten-182 ( $^{182}\text{W}$ ) with a half life of 9 Myr. The decay of  $^{182}\text{Hf}$  in the martian mantle after removal of W in the core resulted in the production of excess radiogenic  $^{182}\text{W}$  compared to other isotopes of W in chondrites. The  $^{182}\text{W}$  excess in the martian mantle is known from measurements of shergottite-nakhlite-chassignite (SNC) meteorites that are thought to have been ejected from Mars by impactors (*e.g.*, Kleine et al. 2004, 2009; Foley et al. 2005; Dauphas and Pourmand 2011). Strictly speaking,  $^{182}\text{W}$  variations record the timing of core formation but this process presumably tracked planetary accretion. In this contribution, we use  $^{182}\text{W}$  excess in the martian mantle and the mass of Mars to constrain the disk surface density and initial planetesimal size in the Mars-forming region.

## 2. MARS FORMATION

We use the following disk model for the initial surface mass density of planetesimals  $\Sigma_{\text{s},0}$  and gas  $\Sigma_{\text{g},0}$ :

$$\Sigma_{\text{s},0} = x\Sigma_{\text{MMSN},\text{s}} \left( \frac{a}{1\text{AU}} \right)^{-3/2} \text{ g cm}^{-2}, \quad (1)$$

$$\Sigma_{\text{gas},0} = x\Sigma_{\text{MMSN},\text{g}} \left( \frac{a}{1\text{AU}} \right)^{-3/2} \text{ g cm}^{-2}, \quad (2)$$

where  $\Sigma_{\text{MMSN},s} = 7.1 \text{ g cm}^{-2}$  and  $\Sigma_{\text{MMSN},g} = 1.7 \times 10^3 \text{ g cm}^{-2}$  are, respectively, the solid and gas surface densities at 1 AU in the minimum-mass solar nebula (MMSN) model (Hayashi 1981), and  $a$  is the distance from the Sun. We vary the scaling factor  $x$  to investigate the conditions for Mars formation. The solid surface density evolves naturally in the simulation, while the gas density is artificially imposed to decrease as a function of time as  $\exp(-t/\tau_d)$  with a gas dissipation timescale  $\tau_d$ . Disk observations indicate that  $\tau_d$  is on the order of several million years (Haisch et al. 2001).

Kobayashi et al. (2010, 2011) showed that model outputs of statistical simulations of runaway and oligarchic growth are controlled primarily by the planetesimals that dominate the initial solid surface density, so the results are largely insensitive to the initial size distribution of other minor bodies. For this reason, we have adopted a fixed initial planetesimal radius  $r_0$  rather than using an actual initial size distribution, which is poorly known anyhow (Morbidelli et al. 2009; Weidenschilling 2011). We limit our analysis to  $r_0 \geq 1 \text{ km}$  because in a turbulent disk, smaller planetesimals would not be sensitive to gravitational focusing, thus preventing runaway growth to proceed (e.g., Youdin and Lithwick 2007; Ormel and Cuzzi 2007; Ormel et al. 2010).

We performed numerical simulations of Mars formation via collisional evolution of planetesimals. In the model, the disk is divided into four annuli. The width of each annulus is given by 0.2 times the annulus' characteristic radius defined by the mean of the inner and outer radii of the annulus. The characteristic radii of the annuli are set to 1.5, 1.8, 2.2, and 2.7 AU. Kobayashi et al. (2010, 2011) showed that because the timescale for dust removal by gas drag is much shorter than the timescale for embryo growth, considering a larger disk did not change significantly the final embryo mass. The mass distribution of bodies in each annulus is treated as discrete mass batches with the mass ratio between adjacent mass batches fixed at 1.2. We follow the evolution of the mass distribution via collisions between

bodies. The collisional rates depend on the relative velocities between colliders, which depend on their eccentricities and inclinations. The mass distribution affects eccentricities and inclinations by collisionless interaction between bodies. We therefore calculate the mass and velocity evolution simultaneously, applying the collision rates (Inaba et al. 2001) and the velocity evolution rates due to mutual interactions of bodies (Ohtsuki et al. 2002) and due to gas drag (Adachi et al. 1976). We do not treat collisions and collisionless interactions between bodies in different annuli and therefore adopt an annulus width larger than the feeding zones of planetary embryos. The total fragment mass ejected by a single impact between colliders with masses  $m_1$  and  $m_2$  is assumed to be  $(m_1 + m_2)\phi/(1 + \phi)$  using the dimensionless impact energy  $\phi = m_1 m_2 v^2 / 2(m_1 + m_2)^2 Q_D^*$  (Kobayashi and Tanaka 2010; Kobayashi et al. 2010), where  $v$  is the collisional velocity between the colliders and  $Q_D^*$  is the specific impact energy ( $\text{erg g}^{-1}$  of impacted material) needed for the ejection of a half-mass of colliders. Hydrodynamic impact simulations give  $Q_D^*$  for 100 km sized or smaller bodies (Benz and Asphaug 1999), while  $Q_D^*$  of bodies with radius  $r \gtrsim 100$  km are determined by the gravitational binding energy (Stewart and Leinhardt 2009). Connecting the two regimes (above and below about 100 km), we express  $Q_D^*$  value of a body with mass  $m$ , radius  $r$ , and density  $\rho$  as  $Q_D^* = Q_{0s}(r/1 \text{ cm})^{\beta_s} + Q_{0g}\rho(r/1 \text{ cm})^{\beta_g} + 2C_{gg}Gm/r$ , where  $G$  is the gravitational constant and  $C_{gg} = 9$  from collisional simulations with distinct element method (Stewart and Leinhardt 2009). Here we use  $Q_{0s} = 3.5 \times 10^7 \text{ erg g}^{-1}$ ,  $Q_{0g} = 0.3 \text{ erg cm}^3 \text{ g}^{-2}$ ,  $\beta_s = -0.38$ , and  $\beta_g = 1.36$ , which were obtained from hydrodynamic simulations for basalt with  $v = 3 \text{ km/s}$  (Benz and Asphaug 1999). Following Wetherill and Stewart (1993) and Inaba et al. (2001), when the bodies reach a certain mass  $m_{\text{run}}$  such that the sum of their mutual Hill radii equals the radial-bin width divided by  $\tilde{b} = 10$  (Kokubo and Ida 2002), the bodies are regarded as “runaway bodies” that do not experience collisions and dynamical interactions due to close encounters among them. Using statistical methods, we can accurately calculate embryo formation and growth until the subsequent stage of

chaotic growth, which may not be significant for Mars. The statistical simulation used in the present contribution reproduces the results of  $N$ -body simulations when collisional fragmentation is ignored (Kobayashi et al. 2010). It also reproduces the analytical solution for mass loss due to a collisional fragmentation cascade (Kobayashi and Tanaka 2010).

Embryos grow via collisions with surrounding planetesimals and fragments. If we assume that the bodies surrounding embryos are not lost at all, then embryos can accrete all the bodies in their feeding zones. The maximum mass of the embryo is called the isolation mass and is given by (e.g., Kokubo and Ida 2002)

$$M_{\text{iso}} = 0.13 x^{3/2} \left( \frac{a}{1.5 \text{ AU}} \right)^{3/4} M_{\oplus}, \quad (3)$$

where we use Eq. (1) for the solid surface density. Therefore, a disk with  $x \sim 1$  produces Mars-size embryos at 1.5 AU if embryos can collect all solids. However, since small planetesimals are vulnerable due to low gravity, mass loss can occur by collisional fragmentation of planetesimals with radial drift of the resulting fragments, so the final embryo mass can be smaller than  $M_{\text{iso}}$ . Destructive collisions between planetesimals produce small bodies, which can in turn be broken apart resulting in still smaller bodies. In the collisional fragmentation cascade, the mass distribution of bodies follows a power law; the surface number density of bodies with mass ranging from  $m$  to  $m + dm$  is proportional to  $m^{-\alpha} dm$ , where  $\alpha = (11 + 3p)/(6 + 3p)$  with  $v^2/Q_{\text{D}}^* \propto m^p$  (Kobayashi and Tanaka 2010). The mass distribution is determined by the collisional cascade for bodies with  $r \lesssim r_0$ , while runaway growth of planetesimals regulates the mass distribution of bodies with  $r \gtrsim r_0$ . With such a mass distribution, planetesimals with radii  $\sim r_0$  determine the solid surface density. The timescale of planetesimal depletion by the collisional fragmentation depends on  $Q_{\text{D}}^*$  of planetesimals and is given by (Kobayashi and Tanaka 2010)

$$\begin{aligned} \tau_{\text{cc}} = & 1.1 \times 10^4 x^{-0.71} \left( \frac{r_0}{10 \text{ km}} \right)^{1.69} \left( \frac{a}{1.5 \text{ AU}} \right)^{3.2} \\ & \times \left( \frac{M}{0.11 M_{\oplus}} \right)^{-0.48} \left( \frac{Q_{0\text{g}}}{0.3 \text{ erg cm}^3 \text{ g}^{-2}} \right)^{-0.72} \text{ yr}, \end{aligned} \quad (4)$$

where we assume that the planetesimal eccentricities are in an equilibrium state controlled by stirring by embryos and damping by gas drag and use  $Q_D^* = Q_{0g}\rho(r_0/1\text{ cm})^{\beta_g}$  with  $\rho = 3\text{ g cm}^{-3}$  for planetesimals. Erosive (cratering) collisions with specific impact energies smaller than  $Q_D^*$  control this timescale (Kobayashi and Tanaka 2010), which is 4–5 times shorter than that derived by ignoring erosive collisions as previous studies did (e.g., Wetherill and Stewart 1993). This timescale was obtained by assuming power law mass distribution in the collision cascade. Several effects can lead to departure from such power-law behavior but this would not change significantly the timescale because it is determined by bodies for which the mass distribution does not deviate considerably from a power-law distribution with  $\alpha \sim 11/6$ . Since  $\tau_{cc}$  is inversely proportional to the solid surface density (Kobayashi and Tanaka 2010),  $\tau_{cc}$  increases with decreasing  $\Sigma_s$  and the full-depletion timescale of planetesimals is much longer than  $\tau_{cc}$ .

The timescale for embryo growth via planetesimal accretion is given by (Kokubo and Ida 2002; Chambers 2006; Kobayashi et al. 2010),

$$\begin{aligned} \tau_{\text{grow,p}} &= 2.7 \times 10^5 x^{-7/5} \left(\frac{r_0}{10\text{ km}}\right)^{2/5} \\ &\times \left(\frac{a}{1.5\text{ AU}}\right)^{27/10} \left(\frac{M}{0.11 M_\oplus}\right)^{1/3} \text{ yr}. \end{aligned} \quad (5)$$

For  $r_0 \gtrsim 100\text{ km}$ , embryos can reach  $M_{\text{iso}}$  in a disk with  $x \approx 1$  because  $\tau_{\text{grow,p}} \lesssim \tau_{cc}$ . However, the final embryo mass is smaller than the isolation mass for  $r_0 \lesssim 100\text{ km}$ . Larger  $x$  is needed for smaller planetesimals to compensate for loss of mass through gas drift of collision fragments and achieve the same final embryo mass. Note that the necessary  $x$  to produce Mars-size embryos is lower than  $x$  given by posing  $\tau_{cc} = \tau_{\text{grow,p}}$ , because  $\tau_{cc}$  and  $\tau_{\text{grow,p}}$  increase when the solid surface density decreases (Kobayashi et al. 2010).

For small values of  $r_0$  ( $\lesssim 1\text{--}10\text{ km}$ ), embryo growth proceeds to a large extent by fragment accretion. The collisional fragmentation cascade halts when eccentricities and inclinations of the bodies are damped well by gas drag. Fragments thus accumulate at

$v^2 \approx 0.5Q_D^*$ . This condition gives a typical fragment size of 1–10 m depending on the embryo mass  $M$ . The radial drift timescale of such bodies is given by (see the derivation in Kobayashi et al. 2010)

$$\begin{aligned} \tau_{\text{drift}} &= \frac{\tau_{\text{stop}}}{2\eta} = \frac{2^{1/3}\pi\tilde{b}Q_D^*}{\eta v_K^2 P_{\text{VS,low}}\Omega_K} \\ &= 6.9 \times 10^2 \left(\frac{a}{1.5 \text{ AU}}\right) \left(\frac{M}{0.11 M_\oplus}\right)^{-1} \\ &\quad \times \left(\frac{Q_D^*}{6.1 \times 10^6 \text{ erg g}^{-1}}\right) \text{yr}, \end{aligned} \tag{6}$$

where  $\Omega_K$  is the Keplerian frequency, we use the value of  $Q_D^*$  for  $r = 1$  m,  $\tau_{\text{stop}}$  is the stopping time by gas drag for the fragments under the Stokes regime,  $v_K$  is the Keplerian velocity,  $P_{\text{VS,low}} = 73$  is the dimensionless viscous stirring rate for low eccentricity, and  $\eta = (v_K - v_{\text{gas}})/v_K$ . Since small fragments have low eccentricities and inclinations, fragment accretion allows fast growth of embryos. The embryo growth timescale via fragment accretion is given by (Kobayashi et al. 2010)

$$\tau_{\text{grow,frag}} = 4.3 \times 10^3 x^{-1} \left(\frac{M}{0.11 M_\oplus}\right)^{1/3} \left(\frac{a}{1.5 \text{ AU}}\right)^2 \text{yr}. \tag{7}$$

If we ignore the radial drift of fragments, embryos reach  $M_{\text{iso}}$  in a short timescale of  $\tau_{\text{grow,frag}}$  (Rafikov 2004; Kenyon and Bromley 2009). However, fragments are removed by radial drift due to gas drag in a shorter timescale of  $\tau_{\text{drift}}$ , which stalls embryo growth before they reach isolation masses. In the case of fragment accretion (small initial planetesimals), formation of Mars-size embryo requires  $\tau_{\text{drift}} \approx \tau_{\text{grow,frag}}$ ;  $x \gtrsim 6$ . With larger initial planetesimals, collisional fragmentation of planetesimals is less effective and therefore embryos can reach the mass of Mars for smaller  $x$ .

To summarize, small initial planetesimals are prone to fragmentation and mass loss occurs through gas-induced drift of fragments. As a result, small planetesimals tend to produce small embryos (and vice versa). The eccentricities and inclinations of fragments

produced by collisions between small planetesimals are damped by interaction with the gas. The resulting reduction in relative velocities increases the gravitational cross section of embryos for fragments, so small planetesimals allow rapid embryo growth (and vice versa).

We start the investigation for embryo growth in a MMSN disk, where the final embryo mass is about the mass of Mars if embryos can fully accrete bodies in their feeding zones;  $M_{\text{iso}} \approx 0.1M_{\oplus}$  at 1.5 AU. Fig. 1a shows the time evolution of planetary embryo masses at 1.5 AU for  $r_0 = 1, 3.7, 27$  and 100 km with  $\tau_d = 10$  Myr. Growth rates and final masses of embryos depend on  $r_0$ . Mars-sized embryos can be formed from planetesimals with  $r_0 \gtrsim 10$  km in the MMSN disk, while a more massive disk is necessary to form Mars from smaller initial planetesimals.

The embryo mass evolution affects the predicted  $^{182}\text{W}$  radiogenic excess caused by the partitioning of W into the core and the decay of  $^{182}\text{Hf}$  in the mantle. In the embryo mantle, the excess abundance of  $^{182}\text{W}$  compared to the chondritic reference value (CHUR = chondritic uniform reservoir) is given by (see the derivation in Appendix A; Jacobsen 2005; Dauphas and Pourmand 2011)

$$\begin{aligned} \varepsilon^{182}\text{W}_{\text{mantle}} &= q_{\text{W}} \left( \frac{^{182}\text{Hf}}{^{180}\text{Hf}} \right) f_{\text{mantle}}^{\text{Hf/W}} \lambda \\ &\times \int_0^t \left( \frac{M(t')}{M(t)} \right)^{1+f_{\text{mantle}}^{\text{Hf/W}}} \exp(-\lambda t') dt', \end{aligned} \quad (8)$$

where  $\varepsilon^{182}\text{W}_{\text{mantle}} = [(^{182}\text{W}/^{184}\text{W})_{\text{mantle}} / (^{182}\text{W}/^{184}\text{W})_{\text{CHUR}} - 1] \times 10^4$ ,  $q_{\text{W}} = (^{180}\text{Hf}/^{182}\text{W})_{\text{CHUR}} \times 10^4$ ,  $f_{\text{mantle}}^{\text{Hf/W}} = (\text{Hf/W})_{\text{mantle}} / (\text{Hf/W})_{\text{CHUR}} - 1$ ,  $M(t)$  is the embryo mass at time  $t$ , and  $\lambda$  is the decay constant of  $^{182}\text{Hf}$ . From previous studies,  $\varepsilon^{182}\text{W}_{\text{Mars mantle}} = 2.68 \pm 0.19$ ,  $f_{\text{Mars mantle}}^{\text{Hf/W}} = 3.38 \pm 0.56$ ,  $q_{\text{W}} = 1.07 \times 10^4$  and  $(^{182}\text{Hf}/^{180}\text{Hf}) = (9.72 \pm 0.44) \times 10^{-5}$  (Dauphas and Pourmand 2011, and references therein). Our simulations generate as model output the time evolution of an embryo mass  $M(t)$ , allowing us to calculate  $\varepsilon^{182}\text{W}_{\text{mantle}}$ . Fig. 1b shows the evolution of  $\varepsilon^{182}\text{W}_{\text{mantle}}$  during

embryo growth with different initial planetesimal radii in the MMSN disk. The predicted  $\varepsilon^{182}\text{W}_{\text{Mars mantle}}$  values are smaller than the measured one for  $r_0 = 1\text{--}100$  km. Small  $r_0$  values produce  $\varepsilon^{182}\text{W}_{\text{mantle}}$  close to the martian mantle value (Fig. 1b) but the final embryo mass is too small and a more massive disk is required (Fig. 1a).

The results for massive disks with  $x = 2.7$  are shown in Fig. 2. Smaller initial planetesimals with  $r_0 = 3.7$  km can make Mars-size embryos, while larger planetesimals make embryos that are much larger than Mars. The predicted  $\varepsilon^{182}\text{W}$  value for  $r_0 = 3.7$  km is about 2.84, which matches the observation. Therefore, a parameter set of  $x \approx 3$  and  $r_0 \approx 4$  km can account for the mass and  $\varepsilon^{182}\text{W}$  value of Mars. For  $x = 2.7$  and  $r_0 = 3.7$  km, the two inner annuli produce 8 Mars mass bodies, while smaller bodies are formed in the outer annuli close to the outer edge of the simulation. The predicted  $\varepsilon^{182}\text{W}$  values of the embryos are similar but slightly lower for embryos formed in the outer disk relative to those formed in the inner disk. In the proposed scenario, one of the embryos becomes Mars while the others accumulate to make Earth and Venus size planets in the subsequent stage of chaotic growth (see §3.2).

To investigate the conditions required for Mars formation, we have evaluated systematically the effects of initial planetesimal size and solar disk mass on the final mass and accretion timescale of embryos in the Mars-forming region. Fig. 3a summarizes the final embryo masses and the  $\varepsilon^{182}\text{W}_{\text{mantle}}$  values derived from 88 simulations at 1.5 AU for a logarithmic grid of  $x \times r_0$ , where  $x = 1, 1.4, 1.9, 2.7, 3.7, 5.2, 7.2, 10$  and  $r_0 = 1, 1.9, 3.7, 7.2, 14, 27, 52, 100, 190, 370, 720$  km. Final embryo masses reach the mass of Mars on the thick solid curve in the  $x$  and  $r_0$  space of Fig. 3a. Our statistical simulations present a mass distribution of embryos that spans a factor 4–5 in mass, which is a measure of uncertainty in the predicted embryo mass (thin solid curves). The tendency that small initial planetesimals require a massive disk for the formation of Mars-sized bodies is explained by the analytical

solutions for the final embryo mass derived by Kobayashi et al. (2010). Mass loss due to collisional fragmentation with radial drift of fragments reduces the final mass for small  $r_0$ . The  $\varepsilon^{182}\text{W}_{\text{mantle}} \pm \Delta\varepsilon^{182}\text{W}_{\text{mantle}}$  values are calculated from Eq. (8), where  $\Delta\varepsilon^{182}\text{W}_{\text{mantle}}$  is the error in the predicted  $\varepsilon^{182}\text{W}_{\text{mantle}}$  value calculated by propagating all uncertainties on model parameters. At 1.5 AU, the parameter space that reproduces both the accretion timescale and final mass of Mars is  $r_0 \lesssim 10$  km and  $x \gtrsim 1$ .

To evaluate the robustness of our conclusion, we have carefully investigated the parameters that could affect the mass and accretion timescale of Mars. In particular, the influences of embryo atmospheres and gas drag on accretion dynamics, embryo migration, disk dissipation timescales, and disruption strength of bodies are discussed below.

Fig. 4a shows the results of simulations including the collisional enhancement for capture of small particles by embryos induced by the presence of a planetary atmosphere, with a density profile determined by the atmospheric opacity (Inaba and Ikoma 2003). The parameter space that explains the mass and  $\varepsilon^{182}\text{W}$  of Mars is similar to the case without the collisional enhancement by planetary atmosphere. The reason is that embryos have small atmospheres and the atmospheric effect is negligible for an embryo smaller than Mars (Kobayashi et al. 2011).

As discussed previously, gas can damp velocities of small particles, thus increasing the efficiency of their capture by embryos. Ormel and Klahr (2010) further found that gas can directly affect the collisional cross-sections between embryos and small bodies. While the dissipative nature of gas drag promotes collision, strong particle-gas coupling acts against it by allowing fragments to be carried along with the gas passed the embryo. Fig. 4b illustrates the results of simulations including the collisional cross section affected by gas drag that is derived by Ormel and Klahr (2010). The collisional enhancement is significant only at  $\tau_{\text{stop}} \approx \Omega_{\text{K}}^{-1}$  for Mars-size embryos. Since the typical fragments have radii  $\sim 10$  m

corresponding to  $\tau_{\text{stop}} \gg \Omega_{\text{K}}^{-1}$  (Kobayashi et al. 2010), this collisional enhancement is minor for Mars formation (compare Figs. 3a with 4b).

We additionally investigated how the gas dissipation time  $\tau_{\text{d}}$  affected the accretion history of Mars. The final embryo mass and  $\varepsilon^{182}\text{W}$  value for  $\tau_{\text{d}} = 5$  Myr are almost the same as those for  $\tau_{\text{d}} = 10$  Myr (Fig. 5a). Fig. 5b shows the results for an extremely short gas dissipation time of  $\tau_{\text{d}} = 1$  Myr. The parameter space where the mass and accretion timescale of Mars are reproduced is not very different from that obtained when the dissipation time is set to higher values of 5 or 10 Myr.

Recent studies suggested that terrestrial planets were constructed from a narrow ring between the current orbits of Earth and Venus (0.7 to 1 AU; Morishima et al. 2008; Hansen 2009; Walsh et al. 2011). In this scenario, Mars was likely scattered from around the outer edge of the truncated disk. We thus additionally investigate the possibility of Mars formation at 1 AU by setting the characteristic radii of the innermost and outermost annuli at 1 and 2.7 AU, respectively. Figure 3b shows the final embryo mass and the  $\varepsilon^{182}\text{W}$  value at 1 AU in the  $r_0$  and  $x$  space. The parameter space required for the production of Mars-sized embryo is similar to the case at 1.5 AU. However, larger planetesimals with  $r_0 \lesssim 40$  km could explain the mass and accretion timescale of Mars.

A very important development of this work and other recent studies (Kobayashi and Tanaka 2010; Kobayashi et al. 2010) is the recognition that erosive collisions and fragment accretion dominate embryo growth. The treatment of fragmentation depends on  $Q_{\text{D}}^*$ , which affects final embryo masses (Kobayashi et al. 2010, 2011; Bromley and Kenyon 2011). The  $Q_{\text{D}}^*$  value is uncertain. For instance, bodies made of rubble piles have  $Q_{\text{D}}^*$  smaller than what we used, thus producing smaller embryos (Kobayashi et al. 2010). With  $r_0 \lesssim 10$  km, low  $Q_{\text{D}}^*$  requires larger  $x$  for Mars formation, which may rise the value of plausible initial planetesimal radii only slightly.

### 3. Discussion

#### 3.1. Comparison with previous studies

Terrestrial planet formation was investigated by  $N$ -body simulations (Kokubo and Ida 1998, 2000; Morishima et al. 2012). Our statistical simulation does not follow the orbits of bodies individually, but reproduces well the mass and random-velocity evolution obtained from  $N$ -body simulations under the assumption of perfect accretion (Kobayashi et al. 2010).

For terrestrial planet formation, Wetherill and Stewart (1993) performed statistical simulations similar to ours and obtained embryos of mass  $\sim 3 \times 10^{26}$  g after about 0.1 Myr for  $x \approx 2$  and  $r_0 \approx 7$  km, which is slightly larger than embryo masses from our simulations ( $\sim 2 \times 10^{26}$  g). Using the fragmentation model of Wetherill and Stewart (1993), Kenyon and Bromley (2004) carried out statistical simulations for  $r_0 \lesssim 1$  km and obtained embryos of mass about  $5 \times 10^{26}$  g at 1 Myr for  $x \approx 2$ . In our simulations, the embryo masses are of about  $2 \times 10^{26}$  g at 1 Myr for  $x \approx 2$  and  $r_0 = 1$  km. Thus, the final embryo masses predicted in our simulations are systematically lower than those obtained by previous workers for the same sets of conditions. The difference stems from a different treatment of erosive (cratering) collisions. In the fragmentation model of Wetherill and Stewart (1993), erosive collisions with specific impact energies smaller than  $Q_D^*$  yield less ejecta than those that are expected from impact laboratory experiments, while these are well reproduced by the fragmentation model developed by Kobayashi and Tanaka (2010), which is used in the present contribution.

Weidenschilling (2008) carried out simulations of terrestrial planet formation where planetary embryos were treated as individual entities, while small bodies were followed using mass bins. These simulations showed that smaller initial planetesimals produced smaller planetary embryos. This tendency is consistent with ours. Chambers (2008) used

a similar model; starting from planetary embryos and planetesimals. The simulations in Chambers (2008) followed collisional fragmentation cascades using mass bins with a mass ratio between adjacent bins of 10. These wide mass bins artificially slowed down planetesimal depletion by the fragmentation cascade by a factor of  $\sim 4$ . Weidenschilling (2008) and Chambers (2008) considered the migration of embryos due to tidal interaction with the nebula (type I migration; e.g., Tanaka et al. 2002). We briefly discuss the effect of type I migration on terrestrial planet growth below.

### 3.2. Subsequent Evolution of Mars

From our simulations, tens of Mars size embryos with orbital separation of 10 mutual Hill radii are expected to form in the terrestrial planet forming region. For Mars to remain small during chaotic growth, Morishima et al. (2008) and Hansen (2009) suggested that planetary embryos must have been concentrated inside about 1 AU. Such orbital concentration may be attained by type I migration of embryos caused by gravitational interaction with the surrounding nebula (e.g., Tanaka et al. 2002) if the torque cancellation due to the unsaturation of corotation torque occurs at  $\lesssim 1$  AU where heating by disk accretion determines disk temperature (Paardekooper et al. 2010, 2011; Kretke and Lin 2012). Mars may have evaded collisions with other embryos during chaotic growth by being scattered to its current orbit at 1.5 AU. The planets resulting from simulations of chaotic growth have orbital eccentricities higher than those of Venus and Earth (Chambers et al. 1996), but these eccentricities were most likely damped by gravitational interactions with a tenuous gas disk and/or a planetesimal swarm (Kominami and Ida 2002; O’Brien et al. 2006; Morishima et al. 2008). This dynamical friction could have been achieved by small ( $\lesssim 10$  m) leftover planetesimals that were accreted by Earth and Mars after completion of core formation (Schlichting et al. 2012). The mass of the late veneer on Mars is estimated

from abundances of highly siderophile elements in SNC meteorites to be  $\sim 1.6 \times 10^{24}$  g. Assuming a chondritic impactor composition ( $\sim 100 \text{ ng g}^{-1}$ ; Wasson and Kallemeyn 1988), this would have delivered  $\sim 1.6 \times 10^{17}$  g of W (Warren 1999; Walker 2009). The martian mantle contains  $\sim 3.2 \times 10^{19}$  g of W (62 ppb W; Lodders and Fegley 1997). Thus, planetesimals responsible for damping the eccentricities and inclinations of the terrestrial planets may have delivered only  $\sim 0.5\%$  of the W inventory of the martian mantle and would have had a negligible effect on the W isotopic composition.

Walsh et al. (2011) proposed that Jupiter migrated inward until Saturn was caught in a 2:3 resonance with Jupiter, at which point Jupiter migrated outwards. The U-turn migration of Jupiter at 1.5 AU would have truncated the disk and could explain Mars present orbit and mass. If the Jupiter’s passing fully cleaned up small bodies, proto-Mars could no longer grow after it was scattered to the current orbit. Our simulations can be interpreted in light of this scenario by considering Mars’ isolation time  $\tau_i$ , after which the embryo stops growing. The U-turn migration of Jupiter occurred at  $\tau_d$  (Walsh et al. 2011). Proto-Mars could be scattered to its current orbit after the migration of Jupiter;  $\tau_i \gtrsim \tau_d$ . For  $\tau_i \gtrsim 20 \text{ Myr}$  – several times longer than the gas dissipation time  $\tau_d$ , Mars’ small mass and rapid accretion is best explained by starting with small planetesimals as was discussed above (Fig. 6a). However, if one considers a rapid isolation time, which is more likely in the context of the Grand Tack scenario (Walsh et al. 2011), models that start with large planetesimals are allowed (Fig. 6b), because Mars avoids late accretion of chondritic material. As discussed in Sect. 3.3, considering the conditions needed to form Jupiter and Saturn, the scenario of formation of Mars from large planetesimals in a MMSN disk is unlikely.

A standing question is whether collisions between Mars and other embryos during chaotic growth could have lead to further growth and modified the W isotope evolution

of the martian mantle. During such collisions, the core of the impactor may partially merge with the target core without complete isotopic equilibration with the target mantle (Dahl and Stevenson 2010). Therefore Mars growth via collisions of sub-Mars embryos in the subsequent stage of chaotic growth might be allowed to some extent. However, a planetesimal disk leading to small embryos would not have contained enough mass to produce the terrestrial planets, which makes it unlikely that Mars grew by the protracted accretion of small embryos.

Mars has experienced at least one collision at a later stage. The northern hemisphere of Mars is lower and has thinner crust than the southern hemisphere, a feature that is commonly referred to as the martian hemispheric dichotomy. Several interpretations have been proposed, including one that calls for a large impact that would have obliterated the northern hemisphere less than 100 Myr after Solar System formation (e.g., Wilhelms and Squyres 1984; Andrews-Hanna et al. 2008; Marinova et al. 2008; Nimmo et al. 2008). Marinova et al. (2008) used smooth particle hydrodynamics simulations to constrain the impactor to a 1,000 km-radius body that would have impacted Mars at a  $\sim 45^\circ$  angle. Using the mass-radius relationship  $R/R_\oplus = (M/M_\oplus)^{0.306}$  ( $R_\oplus$  is Earth radius; Sotin et al. 2007), such an impactor would have delivered  $\approx 2\%$  of the mass of Mars. Most likely, this would have taken place after most  $^{182}\text{Hf}$  had decayed, possibly  $\approx 50$  Myr after solar system formation. We have evaluated the impact of such a late impact on the W isotopic evolution of the martian mantle for one of the simulations that reproduces the mass and  $\varepsilon^{182}\text{W}$  values of Mars ( $x = 2.7$  and  $r_0 = 3.7$  km). The calculated  $\varepsilon^{182}\text{W}$  shifts from 2.7 to 2.5 when taking into account this late impactor. This is well within uncertainties, so our conclusions are not affected by the possibility that the martian dichotomy was produced by a late impactor. The assumption of a 1000-km radius body is conservative as Nimmo et al. (2008) considered a head on collision with a smaller body of 320 km radius, which would have a negligible effect on  $\varepsilon^{182}\text{W}$ .

### 3.3. Radial Gradient of planetesimal sizes

As discussed in §3.2, two scenarios can explain the small mass and  $\varepsilon^{182}\text{W}$  value of Mars: (i) small planetesimals in a massive disk formed Mars or (ii) large planetesimals in an  $\sim\text{MMSN}$  disk formed Mars but its growth was arrested early by inward then outward migration of Jupiter. Further constraints bearing on this issue can be obtained by examining the conditions necessary for giant planet formation. If an embryo reaches a critical core mass, it cannot sustain a static atmosphere and starts rapid gas accretion to form a gas giant planet, such as Jupiter and Saturn (e.g., Mizuno 1980; Ikoma et al. 2000). However, before the embryo attains the critical core mass, collisional fragmentation induced by gravitational stirring stalls the growth of the embryo (Kobayashi et al. 2010). Inaba et al. (2003) suggested that fragment accretion enhanced by tenuous atmospheres allowed formation of massive cores. Levison et al. (2010) meanwhile pointed out that combination of gas drag and stirring by an embryo inhibits the accretion of fragments with radii larger than 30 m onto the embryo. However, the typical fragment radius is smaller than 30 m and hence the obstacle to fragment accretion is negligible (see the discussion in Kobayashi et al. 2010). Since the removal of fragments due to radial drift is more effective than accretion, embryos cannot reach the critical core mass starting from small initial planetesimals. Although the core formation must be completed before gas depletion, the formation timescale of a core is longer than  $\tau_d$  for large planetesimals, for which initial runaway growth or cores is slow. Therefore, Jupiter’s core is likely to have formed from accretion of intermediate size planetesimals in a massive disk (Kobayashi et al. 2011).

Jupiter’s gas accretion was truncated by its gap opening. At the edge of the gap, a radial pressure maximum was created. Small fragments accumulated at the pressure maximum, which might have lead to the formation of Saturn’s core in  $\sim 10^6\text{yr}$  (Kobayashi et al. 2012). Heat released by solid accretion stabilizes atmospheres of cores and delays the

rapid gas accretion to form gas giant planets, and hence high solid accretion rates of cores result in large cores (e.g., Ikoma et al. 2000). Saturn’s core is estimated to be larger than Jupiter’s core (Saumon and Guillot 2004), which is difficult to explain in classical core formation models. Lambrechts and Johansen (2012) recently proposed a core formation scenario by accretion of sub-meter sized pebble, which also produces a higher accretion rate for Jupiter unless the pebble surface density has a flat radial profile (the radial slope  $d \ln \Sigma_s / d \ln a > -0.5$ ). A promising model to explain Saturn’s large core relative to Jupiter is if Saturn’s core was formed at the gap opened by Jupiter (Kobayashi et al. 2012).

In the context of the model of Kobayashi et al. (2011, 2012), which uses the same prescriptions as used in the present contribution, Jupiter and Saturn can be formed in limited conditions for planetesimal sizes and disk masses. Large planetesimals  $r_0 \approx 30$ –200 km in a massive disk  $x \gtrsim 3$  are required to form a massive core of  $5M_\oplus$  at 5.2 AU for Jupiter (Kobayashi et al. 2011). On the other hand, the larger core of Saturn requires very rapid formation, which is realized by fragment accretion at the pressure maximum caused by Jupiter’s gap opening in the solar nebula. This yields an additional constraint described empirically by the relationship  $x \gtrsim \sqrt{r_0/1 \text{ km}}$  (Kobayashi et al. 2012). Both conditions for formation of the cores of Jupiter and Saturn are satisfied for  $x \gtrsim 7$  and  $r_0 \approx 30$ –100 km (see Fig. 3).

As shown in Figs. 3–6, the conditions required to explain the accretion of the cores of Jupiter and Saturn are inconsistent with those inferred for Mars. The condition required for Jupiter and Saturn formation produces Earth-sized or larger embryos in the terrestrial planet region and the predicted  $\varepsilon^{182}W_{\text{mantle}}$  adopting  $f_{\text{mantle}}^{\text{Hf/W}} = 12$  for Earth’s mantle is  $\gtrsim 10$ , which is much larger than  $\varepsilon^{182}W_{\text{mantle}} = 1.85$  in terrestrial rocks (Jacobsen 2005; Kleine et al. 2009; Dauphas and Chaussidon 2011).

One way to try to reconcile the apparently inconsistent conditions inferred for Mars

on the one hand and Jupiter and Saturn on the other hand is to modify the disk surface density. In the discussion above and in Fig. 3–6, we assumed  $\Sigma_g \propto \Sigma_s \propto a^{-1.5}$ . It is possible for instance that the disk surface density had a shallower radial slope of  $\Sigma_g \propto \Sigma_s \propto a^{-1}$ . The conditions for forming the cores of Jupiter and Saturn become  $x \gtrsim 2.4$  and  $r_0 \gtrsim 40$  km. If we use a massive disk of 0.1 solar mass required by Jupiter formation, the radius of initial planetesimals for Mars formation becomes less than 5 km for  $\Sigma_g \propto \Sigma_s \propto a^{-1}$ . Changing the disk density profile does not seem to solve the discrepancy that exists between Mars and the giant planets.

A way to reconcile the constraints derived from inner and outer solar system bodies is if planets formed in a relatively massive solar nebula ( $x \gtrsim 5$ ) but planetesimals sizes were different in the inner and outer regions. In this scenario, Jupiter and Saturn cores would have formed from planetesimals of 50 km radius while Mars formed from smaller planetesimals of  $\lesssim 10$  km radius. Morbidelli et al. (2009) proposed that 100 km or larger planetesimals were necessary to explain the mass distribution of asteroids in the main belt, but Weidenschilling (2011) concluded that planetesimals of 100 m size could also reproduce the asteroid mass distribution. The sizes of planetesimals are related to their formation mechanisms (*e.g.*, Okuzumi et al. 2012; Johansen et al. 2006). The heliocentric gradient in planetesimal sizes discussed here may be related to the inferred contrast in solid surface densities and material properties across the snow line.

We thank D. Minton, A. Morbidelli, and an anonymous reviewer for comments that helped improve the manuscript. HK gratefully acknowledges the support from Grants-in-Aid from MEXT (23103005) and "Institutional Program for Young Researcher Overseas Visits" (R29). ND acknowledges the support of NASA (NNX12AH60G) and NSF (EAR-0820807).

### A. Derivation of $\varepsilon^{182}\text{W}$ evolution

The mantle  $^{182}\text{W}$  value evolves due to extraterrestrial delivery, removal of metal to core, and radioactive decay of  $^{182}\text{Hf}$ . A planetary embryo mainly grows through collisions with small bodies. If the sizes of bodies are much smaller than the thickness of the embryo mantle, the sinking metal breaks up in tiny droplets that can equilibrate isotropically with the surrounding mantle (Rubie et al. 2003; Samuel 2012). On the other hand, one third of embryo mass growth is provided by collisions with similar mass bodies (Chambers 2006; Kobayashi et al. 2010, 2011). According to Morishima et al. (2012), contribution of large bodies to the  $\varepsilon^{182}\text{W}$  evolution of the martian mantle is negligible. Therefore, we assume that the bodies accreted by Mars are fully equilibrated with the mantle before metal removal into the core. Accordingly, the equation governing the  $^{182}\text{W}$  isotopic evolution is,

$$\frac{d}{dt}(M_{\text{mantle}} [^{182}\text{W}]_{\text{mantle}}) = [^{182}\text{W}]_{\text{CHUR}} \frac{dM}{dt} - D^{\text{W}} [^{182}\text{W}]_{\text{mantle}} \frac{dM_{\text{core}}}{dt} + \lambda [^{182}\text{Hf}]_{\text{mantle}} M_{\text{mantle}}, \quad (\text{A1})$$

where  $M_{\text{mantle}}$  and  $M_{\text{core}}$  are, respectively, the mantle and core masses ( $M = M_{\text{mantle}} + M_{\text{core}}$ ),  $D^{\text{W}}$  is the W metal/silicate partition coefficient. The mass balance for W in the bulk planet can be written as,

$$[\text{W}]_{\text{mantle}} M_{\text{mantle}} + D^{\text{W}} [\text{W}]_{\text{mantle}} M_{\text{core}} = [\text{W}]_{\text{CHUR}} M. \quad (\text{A2})$$

On the other hand, Hf does not go to the mantle and the mass balance is given by

$$[\text{Hf}]_{\text{mantle}} M_{\text{mantle}} = [\text{Hf}]_{\text{CHUR}} M. \quad (\text{A3})$$

We assume that the core mass fraction,  $\gamma = M_{\text{core}}/M$ , is constant. We then obtain, from Eqs. (A2) and (A3),

$$f_{\text{mantle}}^{\text{Hf/W}} \equiv \frac{(\text{Hf/W})_{\text{mantle}}}{(\text{Hf/W})_{\text{CHUR}}} - 1 = \frac{D^{\text{W}} \gamma}{1 - \gamma}. \quad (\text{A4})$$

The variation of  $R_{\text{m}} = (^{182}\text{W}/^{184}\text{W})_{\text{mantle}}$  and  $R_{\text{CHUR}} = (^{182}\text{W}/^{184}\text{W})_{\text{CHUR}}$  is given by

Eq. (A1) divided by  $^{184}\text{W}_{\text{mantle}}M$  using Eqs. (A2):

$$(1 - \gamma) \left( R_m \frac{d \ln M}{dt} + \frac{dR_m}{dt} \right) = (1 - \gamma + D^{\text{W}}\gamma) R_{\text{CHUR}} \frac{d \ln M}{dt} - D^{\text{W}}\gamma R_m \frac{d \ln M}{dt} + \lambda(1 - \gamma) \left( \frac{^{182}\text{Hf}}{^{184}\text{W}} \right)_{\text{mantle}}. \quad (\text{A5})$$

Using Eq. (A4) and  $(^{182}\text{Hf}/^{182}\text{W})_{\text{mantle}} = (1 + f_{\text{mantle}}^{\text{Hf/W}})(^{182}\text{Hf}/^{182}\text{W})_{\text{CHUR}}$  and  $dR_{\text{CHUR}}/dt = \lambda(^{182}\text{Hf}/^{184}\text{W})_{\text{CHUR}}$ , we then have

$$\frac{d}{dt}(R_m - R_{\text{CHUR}}) = -(f_{\text{mantle}}^{\text{Hf/W}} + 1)(R_m - R_{\text{CHUR}}) \frac{d \ln M}{dt} + \lambda f_{\text{mantle}}^{\text{Hf/W}} \left( \frac{^{182}\text{Hf}}{^{184}\text{W}} \right)_{\text{CHUR}}. \quad (\text{A6})$$

Integration of Eq. (A6) results in

$$R_m - R_{\text{CHUR}} = \lambda f_{\text{mantle}}^{\text{Hf/W}} \left( \frac{^{182}\text{Hf}}{^{184}\text{W}} \right)_{\text{CHUR},0} \int_0^t \left( \frac{M(t')}{M(t)} \right)^{1+f_{\text{mantle}}^{\text{Hf/W}}} dt'. \quad (\text{A7})$$

Applying the definition of  $\varepsilon^{182}\text{W}$ , Eq. (A7) can be rewritten as Eq. (8).

## REFERENCES

- Adachi, I., Hayashi, C., Nakazawa, K. 1976. The gas drag effect on the elliptical motion of a solid body in the primordial solar nebula.. *Progress of Theoretical Physics* 56, 1756-1771.
- Andrews-Hanna, J. C., Zuber, M.T., Banerdt, W. B. 2008. The Borealis basin and the origin of the martian crustal dichotomy. *Nature* 453, 1212-1215.
- Benz, W., Asphaug, E. 1999. Catastrophic Disruptions Revisited. *Icarus* 142, 5-20.
- Bromley, B. C., Kenyon, S. J. 2011. Migration of Planets Embedded in a Circumstellar Disk. *The Astrophysical Journal* 735, 29.
- Chambers, J. E. 2006. Planet Formation with Migration. *The Astrophysical Journal* 652, L133-L136.

- Chambers, J. 2008. Oligarchic growth with migration and fragmentation. *Icarus* 198, 256-273.
- Chambers, J. E., Wetherill, G. W., Boss, A. P. 1996. The Stability of Multi-Planet Systems. *Icarus* 119, 261-268.
- Dahl, T. W., Stevenson, D. J. 2010. Turbulent mixing of metal and silicate during planet accretion – And interpretation of the Hf-W chronometer. *Earth and Planetary Science Letters* 295, 177-186.
- Dauphas, N., Pourmand, A. 2011. Hf-W-Th evidence for rapid growth of Mars and its status as a planetary embryo. *Nature* 473, 489-492.
- Dauphas, N., Chaussidon, M. 2011. A perspective from extinct radionuclides on a young stellar object: The Sun and its accretion disk. *Annual Review of Earth and Planetary Sciences* 39, 351-386.
- Foley, C. N., Wadhwa, M., Borg, L. E., Janney, P. E., Hines, R., Grove, T. L. 2005. The early differentiation history of Mars from  $^{182}\text{W}$ - $^{142}\text{Nd}$  isotope systematics in the SNC meteorites. *Geochimica et Cosmochimica Acta* 69, 4557-4571.
- Hansen, B. M. S. 2009. Formation of the Terrestrial Planets from a Narrow Annulus. *The Astrophysical Journal* 703, 1131-1140.
- Hayashi, C. 1981. Structure of the Solar Nebula, Growth and Decay of Magnetic Fields and Effects of Magnetic and Turbulent Viscosities on the Nebula. *Progress of Theoretical Physics Supplement* 70, 35-53.
- Haisch, K. E., Jr., Lada, E. A., Lada, C. J. 2001. Disk Frequencies and Lifetimes in Young Clusters. *The Astrophysical Journal* 553, L153-L156.

- Ikoma, M., Nakazawa, K., Emori, H. 2000. Formation of Giant Planets: Dependences on Core Accretion Rate and Grain Opacity. *The Astrophysical Journal* 537, 1013-1025.
- Inaba, S., Ikoma, M. 2003. Enhanced collisional growth of a protoplanet that has an atmosphere. *Astronomy and Astrophysics* 410, 711-723
- Inaba, S., Wetherill, G. W., Ikoma, M. 2003. Formation of gas giant planets: core accretion models with fragmentation and planetary envelope. *Icarus* 166, 46-62.
- Inaba, S., Tanaka, H., Nakazawa, K., Wetherill, G. W., Kokubo, E. 2001. High-Accuracy Statistical Simulation of Planetary Accretion: II. Comparison with N-Body Simulation. *Icarus* 149, 235-250.
- Iwasaki, K., Tanaka, H., Nakazawa, K., Hiroyuki, E. 2001. The Gas-Drag Effect on the Orbital Instability of a Protoplanet System. *Publications of the Astronomical Society of Japan* 53, 321-329.
- Jacobsen, S. B. 2005. The Hf-W Isotopic System and the Origin of the Earth and Moon. *Annual Review of Earth and Planetary Sciences* 33, 531-570.
- Johansen, A., Klahr, H., Henning, T. 2006. Gravoturbulent Formation of Planetesimals. *Astrophysical Journal* 636, 1121-1134.
- Kleine, T., Mezger, K., Munker, C., Palme, H., Bischoff, A. 2004.  $^{182}\text{Hf}$ - $^{182}\text{W}$  isotope systematics of chondrites, eucrites, and martian meteorites: Chronology of core formation and early mantle differentiation in Vesta and Mars. *Geochimica et Cosmochimica Acta* 68, 2935-2946.
- Kleine, T., Touboul, M., Bourdon, B., Nimmo, F., Mezger, K., Palme, H., Yin, Q.-Z., Jacobsen, S.B., Halliday, A.N. 2009. Hf-W chronometry and the accretion and early

- differentiation of asteroids and terrestrial planets. *Geochimica et Cosmochimica Acta* 73, 5150.
- Kenyon, S. J., Bromley, B. C. 2004. Detecting the Dusty Debris of Terrestrial Planet Formation. *The Astrophysical Journal* 602, L133-L136.
- Kenyon, S. J., Bromley, B. C. 2004. Collisional Cascades in Planetesimal Disks. II. Embedded Planets. *The Astronomical Journal* 127, 513-530.
- Kenyon, S. J., Bromley, B. C. 2006. Terrestrial Planet Formation. I. The Transition from Oligarchic Growth to Chaotic Growth. *The Astronomical Journal* 131, 1837-1850.
- Kenyon, S. J., Bromley, B. C. 2009. Rapid Formation of Icy Super-Earths and the Cores of Gas Giant Planets. *The Astrophysical Journal* 690, L140-L143.
- Kobayashi, H., Ormel, C. W., Ida, S. 2012. Rapid Formation of Saturn after Jupiter Completion. *The Astrophysical Journal* 756, 70.
- Kobayashi, H., Tanaka, H. 2010. Fragmentation model dependence of collision cascades. *Icarus* 206, 735-746.
- Kobayashi, H., Tanaka, H., Krivov, A. V. 2011. Planetary Core Formation with Collisional Fragmentation and Atmosphere to Form Gas Giant Planets. *The Astrophysical Journal* 738, 35.
- Kobayashi, H., Tanaka, H., Krivov, A. V., Inaba, S. 2010. Planetary growth with collisional fragmentation and gas drag. *Icarus* 209, 836-847.
- Kokubo, E., Ida, S. 1998. Oligarchic Growth of Protoplanets. *Icarus* 131, 171-178.
- Kokubo, E., Ida, S. 2000. Formation of Protoplanets from Planetesimals in the Solar Nebula. *Icarus* 143, 15-27.

- Kokubo, E., Ida, S. 2002. Formation of Protoplanet Systems and Diversity of Planetary Systems. *Astrophysical Journal* 581, 666-680.
- Kominami, J., Ida, S. 2002. The Effect of Tidal Interaction with a Gas Disk on Formation of Terrestrial Planets. *Icarus* 157, 43-56.
- Kretke, K. A., Lin, D. N. C. 2012. The Importance of Disk Structure in Stalling Type I Migration. *The Astrophysical Journal* 755, 74.
- Lambrechts, M., Johansen, A. 2012. Rapid growth of gas-giant cores by pebble accretion. *Astronomy and Astrophysics* 544, A32.
- Levison, H. F., Thommes, E., Duncan, M. J. 2010. Modeling the Formation of Giant Planet Cores. I. Evaluating Key Processes. *The Astronomical Journal* 139, 1297-1314.
- Lodders, K., Fegley, B. 1997. An Oxygen Isotope Model for the Composition of Mars. *Icarus* 126, 373-394.
- Marinova, M. M., Aharonson, O., Asphaug, E. 2008. Mega-impact formation of the Mars hemispheric dichotomy. *Nature* 453, 1216-1219.
- Mizuno, H. 1980. Formation of the Giant Planets. *Progress of Theoretical Physics* 64, 544-557.
- Morbidelli, A., Bottke, W. F., Nesvorný, D., Levison, H. F. 2009. Asteroids were born big. *Icarus* 204, 558-573.
- Morishima, R. Golabek, G. J., Samuel, H. 2012. *N*-body simulations of oligarchic growth of Mars: Implications for Hf-W chronology. *Earth and Planetary Science Letters* 366, 6–16.

- Morishima, R., Schmidt, M. W., Stadel, J., Moore, B. 2008. Formation and Accretion History of Terrestrial Planets from Runaway Growth through to Late Time: Implications for Orbital Eccentricity. *The Astrophysical Journal* 685, 1247-1261.
- Nimmo, F., Hart, S. D., Korycansky, D. G., Agnor, C. B. 2008. Implications of an impact origin for the martian hemispheric dichotomy. *Nature* 453, 1220-1223.
- O'Brien, S., Osborne, S., Buckley, K., Fehse, R., Amann, A., O'Reilly, E. P., Barry, L. P., Anandarajah, P., Patchell, J., O'Gorman, J. 2006. Inverse scattering approach to multiwavelength Fabry-Pérot laser design. *Physical Review A* 74, 063814.
- Ogihara, M., Ida, S., Morbidelli, A. 2007. Accretion of terrestrial planets from oligarchs in a turbulent disk. *Icarus* 188, 522-534.
- Ohtsuki, K., Stewart, G. R., Ida, S. 2002. Evolution of Planetesimal Velocities Based on Three-Body Orbital Integrations and Growth of Protoplanets. *Icarus* 155, 436-453.
- Okuzumi, S., Tanaka, H., Kobayashi, H., Wada, K. 2012. Rapid Coagulation of Porous Dust Aggregates outside the Snow Line: A Pathway to Successful Icy Planetesimal Formation. *The Astrophysical Journal* 752, 106.
- Ormel, C. W., Cuzzi, J. N. 2007. Closed-form expressions for particle relative velocities induced by turbulence. *Astronomy and Astrophysics* 466, 413-420.
- Ormel, C. W., Klahr, H. H. 2010. The effect of gas drag on the growth of protoplanets. Analytical expressions for the accretion of small bodies in laminar disks. *Astronomy and Astrophysics* 520, A43.
- Ormel, C. W., Dullemond, C. P., Spaans, M. 2010. Accretion among preplanetary bodies: The many faces of runaway growth. *Icarus* 210, 507-538.

- Ormel, C. W., Kobayashi, H. 2012. Understanding How Planets Become Massive. I. Description and Validation of a New Toy Model. *The Astrophysical Journal* 747, 115.
- Paardekooper, S.-J., Baruteau, C., Crida, A., Kley, W. 2010. A torque formula for non-isothermal type I planetary migration - I. Unsaturated horseshoe drag. *Monthly Notices of the Royal Astronomical Society* 401, 1950-1964.
- Paardekooper, S.-J., Baruteau, C., Kley, W. 2011. A torque formula for non-isothermal Type I planetary migration - II. Effects of diffusion. *Monthly Notices of the Royal Astronomical Society* 410, 293-303.
- Rafikov, R. R. 2004. Fast Accretion of Small Planetesimals by Protoplanetary Cores. *The Astronomical Journal* 128, 1348-1363.
- Rubie, D. C., Melosh, H. J., Reid, J. E., Liebske, C., Righter, K. 2003. Mechanisms of metal-silicate equilibration in the terrestrial magma ocean. *Earth and Planetary Science Letters* 205, 239-255.
- Samuel, H. 2012. A re-evaluation of metal diapir breakup and equilibration in terrestrial magma oceans. *Earth and Planetary Science Letters* 313, 105-114.
- Saumon, D., Guillot, T. 2004. Shock Compression of Deuterium and the Interiors of Jupiter and Saturn. *The Astrophysical Journal* 609, 1170-1180.
- Schlichting, H. E., Warren, P. H., Yin, Q.-Z. 2012. The Last Stages of Terrestrial Planet Formation: Dynamical Friction and the Late Veneer. *The Astrophysical Journal* 752, 8.
- Sotin, C., Grasset, O., Mocquet, A. 2007. Mass radius curve for extrasolar Earth-like planets and ocean planets. *Icarus* 191, 337-351.

- Stewart, S. T., Leinhardt, Z. M. 2009. Velocity-Dependent Catastrophic Disruption Criteria for Planetesimals. *Astrophysical Journal* 691, L133-L137.
- Tanaka, H., Takeuchi, T., Ward, W. R. 2002. Three-Dimensional Interaction between a Planet and an Isothermal Gaseous Disk. I. Corotation and Lindblad Torques and Planet Migration. *The Astrophysical Journal* 565, 1257-1274.
- Youdin, A. N., Lithwick, Y. 2007. Particle stirring in turbulent gas disks: Including orbital oscillations. *Icarus* 192, 588-604.
- Walker, R. J. 2009. Highly siderophile elements in the Earth, Moon and Mars: Update and implications for planetary accretion and differentiation. *Chemie der Erde / Geochemistry* 69, 101-125.
- Walsh, K. J., Morbidelli, A., Raymond, S. N., O'Brien, D. P., Mandell, A. M. 2011. A low mass for Mars from Jupiter's early gas-driven migration. *Nature* 475, 206-209.
- Warren, P. H., Kallemeyn, G. W., Kyte, F. T. 1999. Origin of planetary cores: Evidence from highly siderophile elements in Martian meteorites. *Geochimica et Cosmochimica Acta* 63, 2105-2122.
- Wasson, J. T., Kallemeyn, G. W. 1988. Compositions of chondrites. *Royal Society of London Philosophical Transactions Series A* 325, 535-544.
- Weidenschilling, S. J. 2008. Accretion of planetary embryos in the inner and outer solar system. *Physica Scripta Volume T* 130, 014021.
- Weidenschilling, S. J. 2011. Initial sizes of planetesimals and accretion of the asteroids. *Icarus* 214, 671-684.
- Weidenschilling, S. J., Spaute, D., Davis, D. R., Marzari, F., Ohtsuki, K. 1997. Accretional Evolution of a Planetesimal Swarm. *Icarus* 128, 429-455.

Wetherill, G. W., Stewart, G. R. 1993. Formation of planetary embryos - Effects of fragmentation, low relative velocity, and independent variation of eccentricity and inclination. *Icarus* 106, 190.

Wilhelms, D. E., Squyres, S. W. 1984. The martian hemispheric dichotomy may be due to a giant impact. *Nature* 309, 138-140.

### Figure Caption

Fig. 1 — (a) Time evolution of embryo mass at 1.5 AU in the MMSN disk ( $x = 1$ ), starting from different planetesimal radii  $r_0$ . The gray dotted line indicates the mass of Mars. (b) Evolution of  $\varepsilon^{182}\text{W}_{\text{mantle}}$  obtained from the mass evolution shown in panel (a). The filled circle and the error bar represent the  $^{182}\text{W}$  excess in the martian mantle,  $\varepsilon^{182}\text{W}_{\text{Mars mantle}}$  (Kleine et al. 2009; Dauphas and Pourmand 2011).

Fig. 2 — Same as Fig. 1 but for  $x = 2.7$ .

Fig. 3 — Constraints from final embryo masses and  $\varepsilon^{182}\text{W}$  on the initial radius of planetesimals,  $r_0$ , at 1.5 AU (a) and 1 AU (b) in the  $x \times \text{MMSN}$  disk. Embryos reach the mass of Mars on the solid curve. The region between the thin curves produces embryos within a factor 2 of the mass of Mars. On the thick dashed curve, the predicted  $\varepsilon^{182}\text{W}_{\text{mantle}}$  values correspond to the mean value obtained from Martian meteorites. The thick dashed curve indicates the parameter space where  $\varepsilon^{182}\text{W}_{\text{mantle,up}} = \varepsilon^{182}\text{W}_{\text{mantle}} + \Delta\varepsilon^{182}\text{W}_{\text{mantle}} = 2.49$ . Below this limit, the accretion timescale of Mars would be too long to explain  $\varepsilon^{182}\text{W}_{\text{mantle}}$  measured in Martian meteorites. The colored region at small  $r_0$  represents the condition satisfying the mass and  $\varepsilon^{182}\text{W}_{\text{mantle}}$  value of Mars and the other at  $r_0 \approx 40\text{--}100$  km indicates

the parameters for the formation of Jupiter and Saturn cores. For reference, the right vertical axis represents the disk mass corresponding to  $x$  in the left axis, assuming that the inner and outer edges of the disk are at 0.4 and 30 AU, respectively.

Fig. 4 — Same as Fig. 3a, but including the accretion enhancement by planetary atmosphere (a) and gas drag (b).

Fig. 5 — Same as Fig. 3a, but for different gas dissipation timescales  $\tau_d = 5$  Myr (a) and 1 Myr(b).

Fig. 6 — Same as Fig. 3b (at 1 AU), but introducing the isolation time of mars,  $\tau_i = 20$  Myr (a), 5 Myr (b), after which Mars does not grow at all.

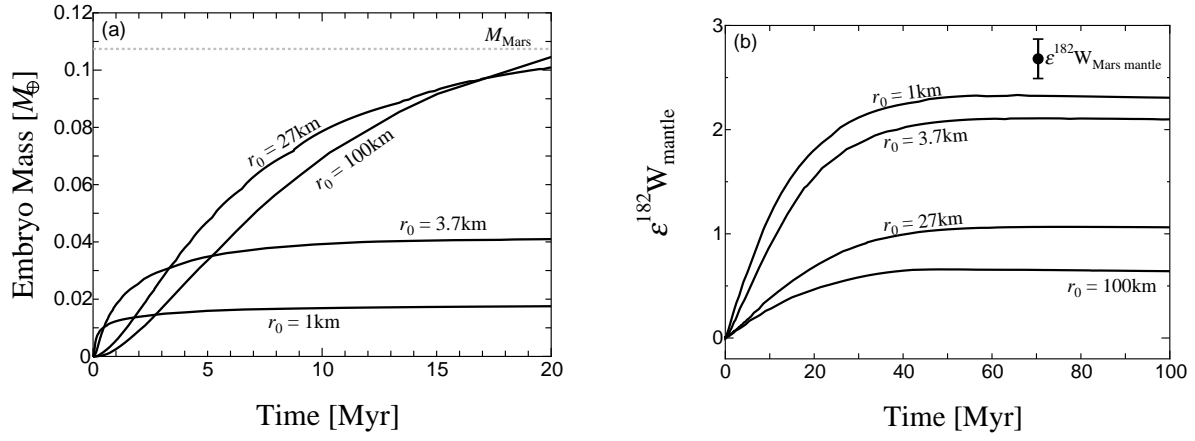


Fig. 1.—

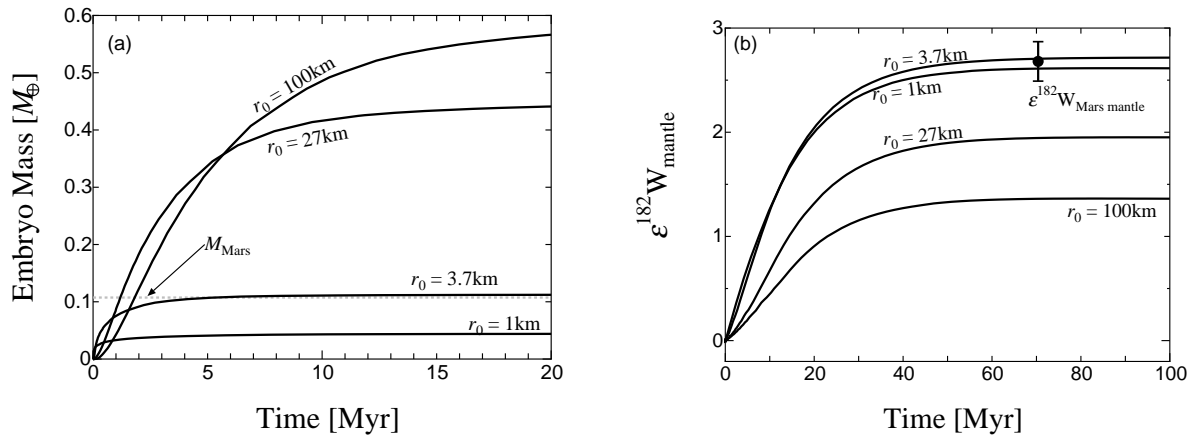


Fig. 2.—

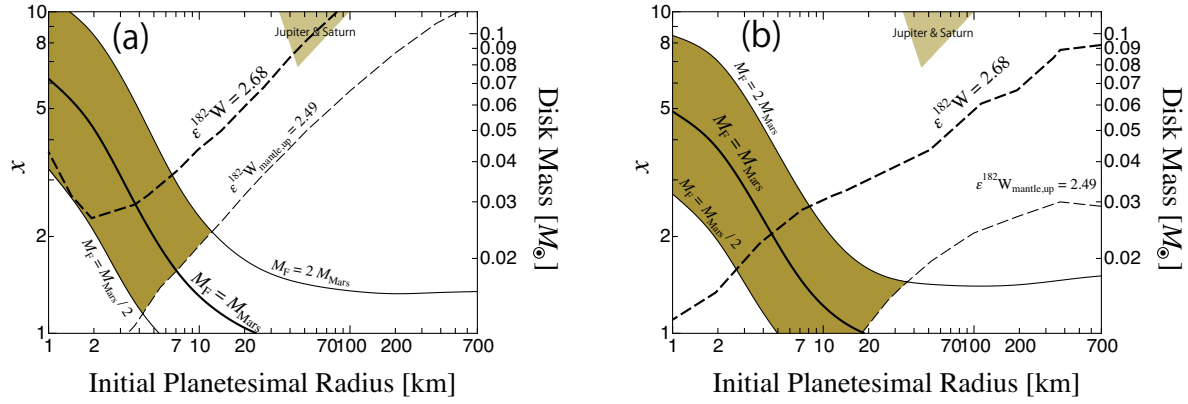


Fig. 3.—

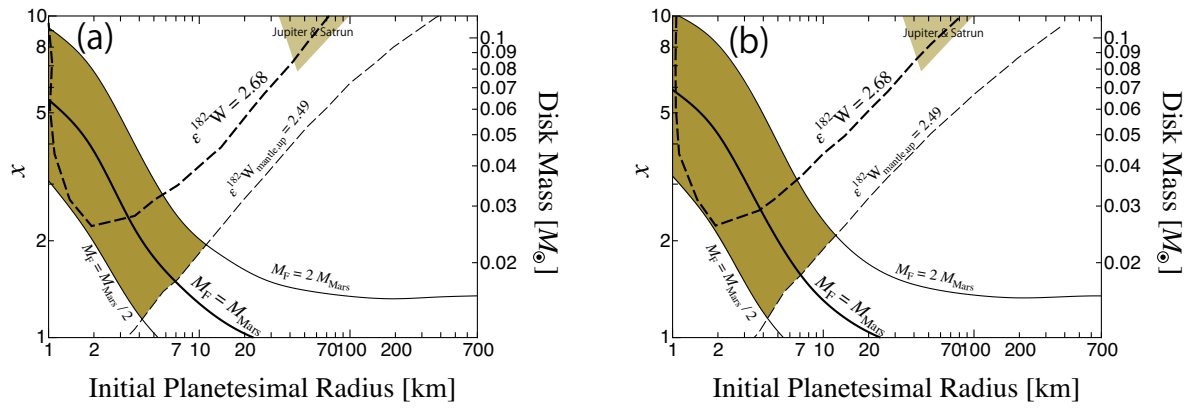


Fig. 4.—

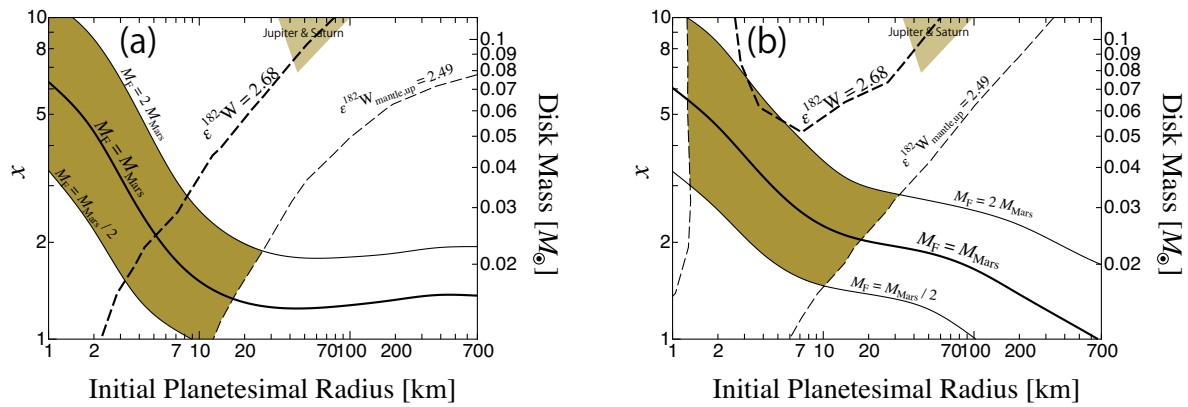


Fig. 5.—

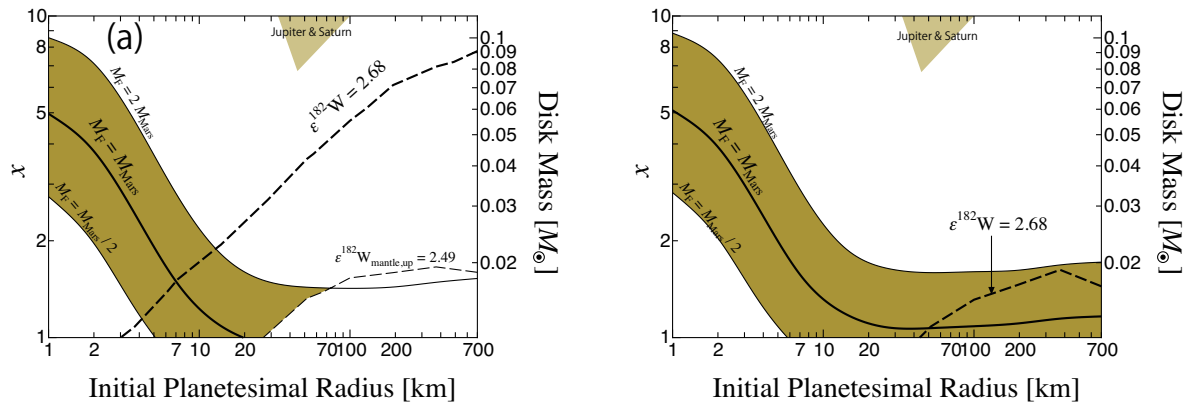


Fig. 6.—